2014 IEEE International Conference on Robotics & Automation (ICRA)
Hong Kong Convention and Exhibition Center
May 31 - June 7, 2014. Hong Kong, China

Automated Microrobotic Characterization of Cell-Cell Communication

J. Liu[1], V. Siragam[2], Z. Gong[1], J. Chen[1], C. Leung[1], Z. Lu[1], C.H. Ru[1], S.R. Xie[1], J. Luo[1], R. Hamilton[2], and Y. Sun[1]

***Abstract*— Most mammalian cells (e.g., cancer cells and cardiomyocytes) adhere to a culturing surface. Compared to robotic injection of suspended cells (e.g., embryos and oocytes), fewer attempts were made to automate the injection of adherent cells due to their smaller size, highly irregular morphology, small thickness (a few micrometers thick), and large variations in thickness across cells. This paper presents a recently developed robotic system for automated microinjection of adherent cells. The system is embedded with several new capabilities: automatically locating micropipette tips; robustly detecting the contact of micropipette tip with cell culturing surface and directly with cell membrane; and precisely compensating for accumulative positioning errors. These new capabilities make it practical to perform adherent cell microinjection truly via computer mouse clicking in front of a computer monitor, on hundreds and thousands of cells per experiment (vs. a few to tens of cells as state-of-the-art). System operation speed, success rate, and cell viability rate were quantitatively evaluated based on robotic microinjection of over 4,000 cells. This paper also reports the use of the new robotic system to perform cell-cell communication studies using large sample sizes. The gap junction function in a cardiac muscle cell line (HL-1 cells), for the first time, was quantified with the system.**

I. INTRODUCTION

Intercellular communication is a critical part of cellular activities and coordinates cell function [1]. Disorders of intercellular communication are responsible for diseases such as cancer [2], autoimmunity [3], and diabetes [4]. A standard technique for measuring intercellular communication is based on monitoring transfer of fluorescent molecules from an individual cell to adjacent cells through functional gap junctions (see Fig. 1). The quantitative measurement of dye transfer requires injection of fluorescent molecules into single cells. In present gap junction testing experiments, only a few or tens of cells can be injected due to the limitations of manual operation, posing a practical hurdle in attaining statistically significant data, for instance, for testing drug molecules on the alteration of gap junction function.

Manually manipulating single cells is tedious and time consuming and has high skill requirements. In manual operation, a skilled operator looks through the eyepieces of a microscope while dexterously controlling multiple devices (e.g., micromanipulators, pump, microscope stage etc.). Robotic cell manipulation technologies progressed significantly over the past decade. The vast majority of demonstrated robotic systems focused on the injection of suspended cells (i.e., oocytes and embryos) [5], [6], [7]. Fewer attempts were made to automate the injection of adherent cells.

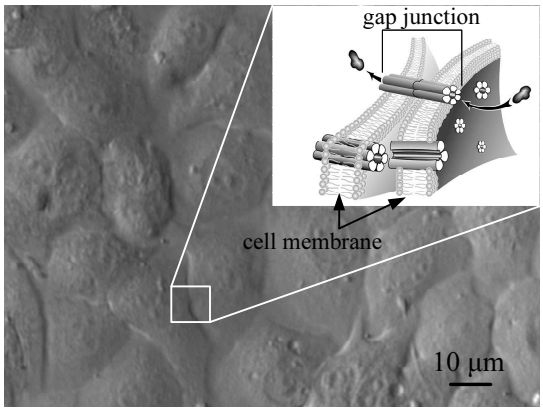

Fig. 1. Adherent cells (HL-1) under 20×. Inset shows the schematic of a gap junction for cell-cell communication.

Most mammalian cells (e.g., cancer cells and cardiomyocytes) adhere to a culturing surface. Different from large suspend cells (e.g., mouse oocytes ∼100 μm; zebrafish embryos ∼1 mm), adherent cells are smaller in size and highly irregular in morphology (vs. spherical for oocytes/embryos), making robust pattern recognition difficult and automation challenging. Additionally, adherent cells are only a few micrometers thick and vary significantly in thickness, posing more stringent requirements in robotic positioning.

A few joystick-based systems were demonstrated to assist operators for adherent cell microinjection [8], [9]. Long training, low success rates, and poor reproducibility make these systems incapable of injecting more than tens of cells per experiment. For example, the most popular commercial system for adherent cell injection is Eppendorf's InjectMan system that requires an operator to look into the eyepieces of a microscope and perform microinjection by controlling joysticks. The injection success rate and cell survival rate of the system are 49.2% and 49.72%, respectively [8]. The only other joystick-based adherent cell injection system was demonstrated for the injection of fluorescent molecules into adherent cell lines with a 49% injection success rate [9]. Due to the difficulty of operating joysticks for fine positioning control, this system does not permit the injection of a high number of cells (only 82 cells injected).

In our previous work in developing robotics technologies for injecting adherent cells [10], we attempted to transform joystick-based operation to computer mouse clicking.

[1]Department of Mechanical and Industrial Engineering, University of Toronto, 5 King's College Road, Toronto, ON M5S 3G8, Canada. sun@mie.utoronto.ca

[2]Division of Cardiology, The Hospital for Sick Children, 555 University Avenue, Toronto, ON M5G 1X8, Canada. robert.hamilton@sickkids.ca

However, several practical limitations in the system required the operator to manually perform a few key steps using joysticks and looking into the eyepieces of the microscope. This hybrid way of system operation (mouse clicking in front of a computer monitor; and operating joysticks under microscope) precluded the system's potential for routine use in biology labs.

Firstly, the system lacked the critical capability for automatically locating a micropipette tip. In adherent cell injection, the micropipette tip must be kept within a few hundreds of nanometers to ensure a high cell viability. Locating the tip under optical microscopy requires high skills and extreme care since tip breakage can easily occur. Additionally, the small tip often gets clogged by large molecules or cell debris, necessitating regular replacement of micropipette tips (e.g., every 100 cells), demanding the system to possess the capability for locating micropipette tip automatically.

The second limitation in our previous system was the limited contact detection capability. In the culturing of adherent cells, cells are more commonly cultured on gels or protein-coated (e.g., collagen) surfaces. Our previously reported contact detection algorithm works well on a bare culturing surface but has a low success rate on these coated surfaces. Furthermore, the previous contact detection algorithm is not applicable when cell confluency (i.e., density) is high (>80%). Thirdly, our previous system was not able to compensate for accumulated positioning errors, which made the system unable to inject more than 100 cells.

In this work, we present a new robotic system capable of injecting thousands of adherent cells. The system successfully addresses the limitations of our previous system prototype [10] and has the following new capabilities: automatically locating micropipette tips; robustly detecting the contact of micropipette tip with cell culturing surface and directly with cell membrane; and precisely compensating for accumulative positioning errors. These new capabilities, for the first time, make it practical to perform adherent cell microinjection truly via computer mouse clicking in front of a computer monitor, making the robotic system suitable for routine use in biology. We also demonstrate the use of the new robotic system to perform cell-cell communication studies using large sample sizes (over 1,000 cells vs. a few to tens of cells as state-of-the-art). Finally, the gap junction function in a cardiac muscle cell line (HL-1 cells), for the first time, was quantified with the new robotic system.

II. SYSTEM OVERVIEW

This system uses well calibrated air pressure to deliver aqueous solution into either the cytoplasm or nucleus of a cell. As shown in Fig. 2(a) and (b), the system consists of a standard inverted microscope (Nikon TE2000-S, Nikon Microscopes) and a motorized X-Y translational stage (ProScan, Prior Scientific, Inc.). The X-Y stage has a travel range of 75 mm along both axes with a resolution of 0.01 μm, a maximum speed of 5 mm/s, and a repeatability of ± 1 μm. A CMOS camera (acA1300-32gm, Basler) is connect to the microscope for visual feedback. A glass capillary,

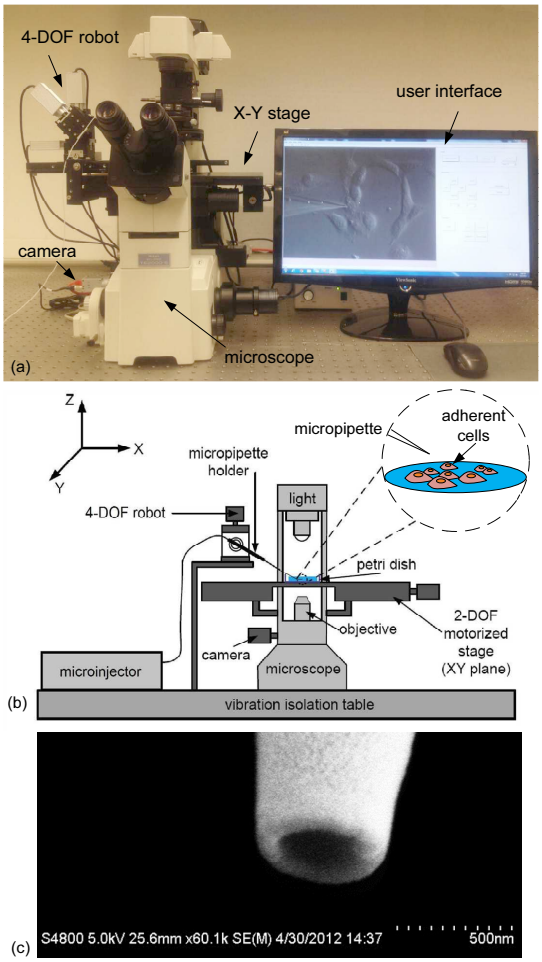

Fig. 2. (a) & (b) Robotic adherent cell injection (RACI) system. (c) Electron microscopy image of micropipette tip.

laser pulled to have an outer diameter of 500 nm and inner diameter of 300 nm [Fig. 2(c)], is mounted to a 4 degrees-of-freedom (DOF) DC-driven micromanipulator (MX7600, Siskiyou, Inc.) that has a travel range of 20 mm and a 0.1 μm positioning resolution along each axis. A host computer executing computer vision microscopy and motion control algorithms controls all hardware.

The robotic micromanipulator and X-Y stage are cooperatively controlled for positioning the micropipette along the XYZ axes and positioning cells in the XY plane. The overall control architecture of the system is summarized in Fig. 3. Microscopy visual feedback is used for providing position feedback to position the micromanipulator and X-Y stage, forming an image-based visual servo control system.

When a micropipette is mounted on the system, the system detects the micropipette tip's position and automatically moves it to the center of the field of view (FOV) [see Section III-A]. The system is capable of contact detection in two modes, either on cell culturing surface or directly on cell membrane [see Section III-B&C], to determine the relative vertical distance between the micropipette tip and the cells in the Z direction. After the injection location (inside cytoplasm or nucleus) on each cell is selected via computer mouse

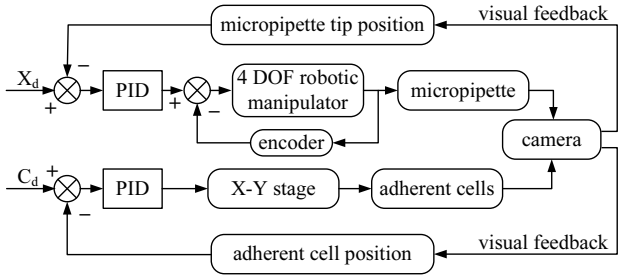

Fig. 3. System control architecture.

clicking, the system controls the micropipette to deliver a precise volume into each cell, and completes the injection of all selected cells following a shortest path. The system then controls the X-Y translational stage to bring cells in the next field of view under microscopy imaging for injection.

III. KEY METHODS

A. Locating Micropipette Tip

When a micropipette tip is mounted on the micromanipulator, the system automatically locates the micropipette tip and moves it to the center of the field of view. This process involves two main steps: micropipette detection and autofocus adjustment.

In the detection step, the micropipette is swept in the X-Y plane for detecting its presence in the field of view. In some cases, the micropipette tip cannot be detected when it is far away from the focal plane. When this occurs, the system moves the focal plane up by controlling the focus adjustment motor, and the X-Y sweep is then repeated. During the sweep of the micropipette, motion history images are generated and used for detecting the presence of the micropipette. The motion history image method is discussed in Section III-C.

In the autofocus step, the system uses the normalized variance method [11] to calculate the focus measure. The autofocus step consists of coarse and fine focus adjustments. Coarse focus adjustment moves the focal plane in a large step size until the entire image produces a maximal focus measure value. In fine focus adjustment, a recursive quad-tree autofocusing method is used to accurately focus on the micropipette tip with smaller step sizes. After the focus adjustments, the in-focus micropipette tip is moved to the center of the field of view through closed-loop visual servoing under a low magnification objective and then under a high magnification objective. The detailed methods for detecting and tracking micropipette tips are described in [12].

B. Contact Detection on Culturing Surface

In order to inject materials into a cell, the relative vertical distance between the micropipette tip and the cell along the Z-direction must be accurately detected. Without the inclusion of an extra sensor (e.g., tactile or force sensors), which increases hardware complexity, two modes of computer vision-based contact detection algorithms are developed to accurately determine the relative heights of the micropipette tip and adherent cells. This section describes the first mode, in which the system detects the initial contact of micropipette tip on the cell culturing surface that is protein coated (vs. bare surface).

1) Empty Region Detection: When cell confluency is lower than 80%, empty areas on the culturing surface [see Fig. 4(a)] can be detected and used for contact detection. The system divides the field of view into sub-regions, the size of which is 100 pixels$\times$100 pixels. The normalized variance of the pixel value, F, is calculated for each region to represent its smoothness, according to

$$F = \frac{1}{W \cdot H \cdot \mu} \sum_{W} \sum_{H} (I(x,y) - \mu)^2 \tag{1}$$

where W and H are the region width and height, $I(x,y)$ is the pixel intensity at the point (x,y), and μ is the average region intensity. This algorithm effectively compensates for differences in average intensity among different regions. The region with the lowest variance value is considered empty and used for performing contact detection.

2) Contact Detection via Three-Dimensional Motion: The system moves the detected empty region in the X-Y plane until it is directly under the micropipette tip. The micropipette tip is lowered by the micromanipulator along the Z direction. When the micropipette tip contacts the bare surface of a Petri dish, further vertical movement of the micropipette tip induces horizontal motion [13]. However, in cell culturing, the Petri dish surface is usually coated with gel or protein (e.g., collagen). The coating makes it difficult for the micropipette tip to 'slide' horizontally (it 'stabs' directly into the coated layer). Therefore, in our new system, the X-Y stage is also servoed simultaneously when the micropipette tip is lowered by the micromanipulator. The X-Y stage's motion enables the reliable generation of the pipette tip's horizontal 'sliding' motion. This results in highly reliable contact detection on protein-coated culturing surfaces.

C. Detection of Contact on Cell Surface

When cell confluency is high, empty regions on the culturing surface becomes unavailable; hence, the system performs contact detection by detecting direct contact of the micropipette tip on the cell surface [see Fig. 4(b)]. After the operator selects a cell via computer mouse clicking, the system moves the cell to the micropipette tip position in the X-Y plane and then moves the micropipette tip downwards along the Z axis. When the micropipette tip contacts the cell surface, the cell is deformed and a subtle motion appears around the contact point. To detect this subtle motion, we developed an algorithm based on motion history images (MHI). The MHI-based method enhances motion representation by accumulating cell deformation over a period of time.

In MHI detection, a region of interest (ROI) is extracted around the micropipette tip [see Fig. 4(c)]. Within the ROI, a mask is applied on top of the micropipette to remove the motion of the micropipette tip [Fig. 4(d)]. When the cell is deformed, a silhouette image is obtained by subtracting two consecutive frames. The silhouette image is then binarized to suppress background noise. When the micropipette continues

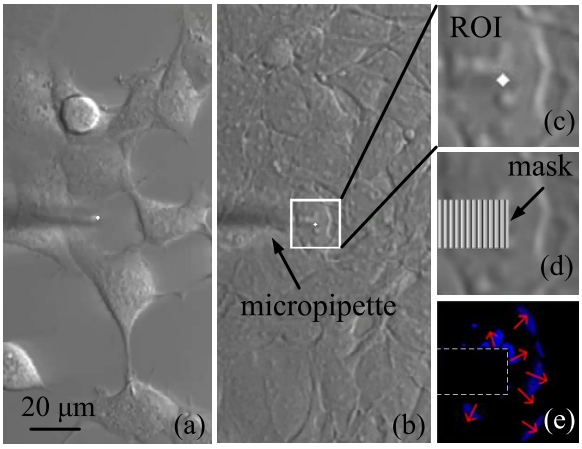

Fig. 4. Contact detection in two modes. (a) When cell confluency is low, the system detects contact of the micropipette tip on the culturing surface. (b) At high cell confluency, the system detects direct contact of the pipette tip on the cell surface. (c) ROI image shows cell being deformed: white dot indicates tip position. (d) Modified ROI removing the motion of micropipette tip. (e) Motion history image showing the deformation of cell: red arrows indicate motion gradients.

to move downwards, new silhouettes of cell deformation are extracted and overlaid to the old silhouette that fades over time. The sequentially fading silhouettes record the motion history of cell's deformation. The MHI, $H_\tau(x,y,t)$, is computed according to

$$H_\tau(x,y,t) = \begin{cases} \tau & \text{if } \Psi(x,y,t)=1 \\ max(0,\ H_\tau(x,y,t-1)-\gamma) & \text{otherwise} \end{cases} \quad (2)$$

where, (x,y) and t represent position and time, the duration τ determines the temporal extent of the movement, γ is the decay parameter, and $\Psi(x,y,t)$ is the binarized image at t. With the MHI-based algorithm, the subtle deforming motion is greatly enhanced by adding the motion history information [see Fig. 4(e)].

The sum of pixel values in MHI, $s(H)$, is calculated as a measure to determine the contact of cell surface. If $s(H)$ is above a threshold value (δ), the micropipette tip is considered as contacting cell top surface. The threshold δ is calculated dynamically by analyzing MHIs in which the micropipette tip has not contacted cell surface.

$$\delta = \bar{s} + a \cdot \sigma(s) \quad (3)$$

where $\bar{s}$ is the average of pixel value sum of the MHIs in which no contact occurs, $\sigma(s)$ is the standard deviation, and a is a preset parameter which determines the threshold value. By adding serval times of standard deviations (i.e., $a \cdot \sigma(s)$) to the mean value, the threshold is able to reject most of the MHIs that do not have cell deformation. Accordingly, false positive detections caused by random noise and the motion of micropipette tip are effectively reduced.

D. Robotic Microinjection

In this new robotic system, an operator performs every step throughout the microinjection process via computer mouse clicking. The operator readily selects injection locations (i.e., cell nucleus or cytoplasm) since the cell nucleus and cytoplasm are distinct on a computer monitor. The operator can select a single cell or multiple cells to inject within the field of view. During computer mouse clicking, cell templates centered at the mouse clicking positions are extracted. The templates are used for template matching to provide position feedback. After performing contact detection, the system moves the micropipette tip close to the first target cell and inserts the micropipette into the target cell along the tilting axis at the maximal speed. The pressure source is then triggered to apply a positive pressure to deposit the preloaded material into the cell. Material deposition results in a "shock wave" motion inside the cell, around the injection location (Fig. 5). The volume of injected materials is precisely controlled by the injection pressure magnitude and width. Although target cells are selected in a random order by the operator, the system injects all cells along the shortest path. The system then moves to the next field of view to continue the injection of more cells. The locations of injected cells are all recorded by the system, permitting time-lapsed imaging of every injected cell.

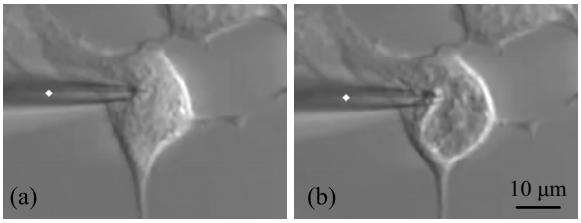

Fig. 5. Robotic injection of adherent cells. When the micropipette is inserted into the cell, material deposition triggered by pressure pulses results in a "shock wave" motion inside the cell.

IV. RESULTS AND DISCUSSION

A. Performance of Locating Micropipette Tip

To evaluate the system's performance of automatically locating micropipette, micropipette tip's initial distance to the culturing surface was divided into five groups. The task of locating micropipette tips in the five groups was also conducted manually by three skilled micromanipulation operators. Experimental results demonstrate that the overall time for auto-locating micropipette tip (30.2s in average) is significantly shorter (p-value<0.001) than in manual operation (averagely 64.8s). Auto-locating micropipette tip was also tested under three imaging modes: bright field, phase contrast, and differential interference contrast (DIC). Although the phase contrast or DIC imaging modes are desired for producing pseudo-3D view of cells, it was found in experiments that bright field imaging produced a high success rate because the micropipette tip appears more uniform and "halo" free under bight field imaging.

B. Injection Speed

Injection speed of the system was evaluated by injecting three different adherent cell lines: HeLa cells, HEK293 cells,

TABLE I

ROBOTIC MICROINJECTION SPEED OF THREE DIFFERENT CELL LINES

cell line	HeLa	HEK293	HL-1	overall
injection number	2281	1068	1116	4465
injection time (min)	97	48	52	197
speed (cells/min)	23.5	22.3	21.5	22.7

TABLE II

INJECTION SUCCESS RATE AND CELL SURVIVAL RATE AFTER INJECTION

injection location	injection number	success rate	survival rate
into cytoplasm	1245	95.2%	97.2%
into nucleus	1036	97.5%	96.5%

and HL-1 cells. The number of injected cells and time consumed are summarized in Table I. The injection time in Table I is the total experimental time for all steps including locating micropipette tip, contact detection, cell selection and injection. The results from the injection of over 4,000 cells show that the injection speed of the robotic system is consistent across different adherent cell lines. The average injection speed is 22.7 cells/min.

C. Injection Success Rate and Cell Survival Rate

The system injected an HPTS fluorescent dye into the cytoplasm or nucleus of HeLa cells. The HPTS dye was chosen because it is highly water-soluble and membrane-impermeable. Therefore, only the cells that are successfully injected with HPTS are able to reveal fluorescent signals. Those cells revealing strong green fluorescent signals were considered as successfully injected. Experimental results summarized in Table II show that the success rates for cytoplasmic (n=1,245) and nuclear (n=1,036) injection were comparable (95.2% and 97.5%).

Cell post-injection viability was evaluated by using a cell viability assay kit (Viability/Cytotoxicity Kit, Life Technologies). The measured cell survival rate after cytoplasmic injection was 97.2% and after nuclear injection was 96.5%.

D. Characterization of Cell-Cell Communication

We used the robotic system to measure gap junction function. In the dye transfer experiments, the membrane-impermeable HPTS dye mixing with Dextran-Rhodamine red dye was injected into a cell. The small fluorescent HPTS molecule (MW=524.37Da) can be transferred from the injected cell to adjacent cells through gap junctions. In contrast, the Dextran-Rhodamine molecule, because of its large molecule size (MW=10,000Da), cannot pass through gap junctions. Therefore, only the injected cell reveal a red fluorescent signal, while the injected cell as well as a number of adjacent cells reveal green fluorescent signal [see Fig. 6]. The exact number of neighboring cells that can reveal green fluorescent signal is determined by the capability of the cells' gap junctions. Thus, intercellular gap junction communication (GJC) was quantitatively investigated by measuring the dye transferred cell number (i.e., the number of cells uptaking fluorescent molecules from the injected cell

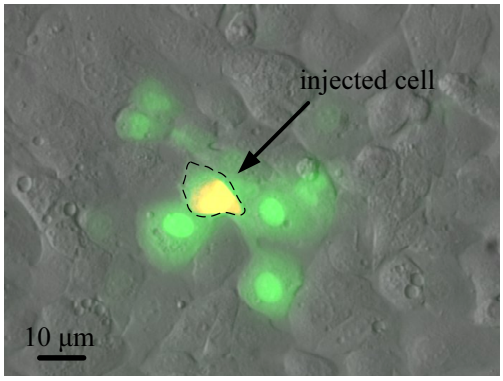

Fig. 6. Only one cell is injected, and fluorescence dye is transferred from the injected cell to adjacent cells through intercellular gap junction communication (GJC).

through gap junctions) and dye transferred distance (i.e., the furthest distance that the fluorescent dye can be transferred).

Gap junction communication was investigated on two different cell lines (i.e., Hela cells, and HL-1 cells). We used 18-α glycyrrhetinic acid (18-αGA) to treat the cells which is known to inhibit the role of GJC in fibroblast growth [14], myoblast fusion [15], and trophoblast proliferation [16]. In our experiments, the robotic system was used to assess GJC of three experiment groups with different doses (25, 50, or 100μM) of 18-αGA treatment. Two control groups were also included. Control group 1 (control 1 in Fig. 7(a)) had no 18-αGA. Since the 18-αGA stocking solution was dissolved in DMSO, a second control group (control 2) with only DMSO treatment was also examined.

The experimental data in Fig. 7(a) shows that there is no significant difference between the two control groups. The number of adjacent cells uptaking fluorescent dye from the injected cells decreased significantly with a higher dose of GJC inhibitor. The results show that 100 μM of 18-αGA effectively blocked almost all the gap junctions for both cell lines. One can also see that HL-1 cells have much higher GJC than Hela cells. HL-1 cell is a cardiac muscle cell line. The strong GJC of HL-1 cells is necessary in impulse propagation in cardiac tissue [17]. The impulse signal is passed efficiently through gap junctions, allowing the cardiac tissue to contract at the same tandem. In contrast, Hela cells, a cancer cell line derived from cervical cancer cells, express little GJC, confirming they do not pass signals via gap junctions for cell coordination. Limited GJC results in poor inhibition of cancer cell mitosis, causing tumor formation [18].

Dye transfer distance was measured, for the first time, for HL-1 cells. Fig. 7(b) shows that a higher dose of 18-αGA inhibitor resulted in significantly shorter dye transfer distances.

E. Discussion

Microinjection of adherent cells permits the direct insertion of foreign materials (e.g., DNA/RNA, fluorescent dyes, quantum dots etc.) into single cells. It is a decades old technology that is still widely used in cell biology for testing cell-cell communication, studying intracellular behavior, and

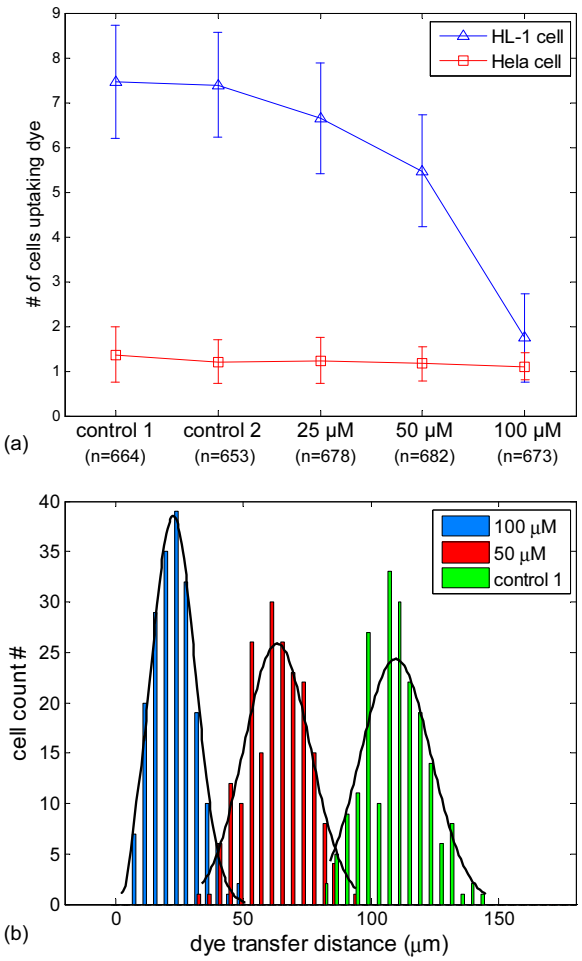

Fig. 7. Results of dye transfer experiments. (a) The number of cells uptaking fluorescence dye from the injected cells. (b) Histogram of dye transfer distance for HL-1 cells.

gene transfection [19].

Manual microinjection of adherent cells and existing robotic system prototypes are limited to the injection of a few to tens of cells per experiment at best. Our new robotic system described in this paper is the first system capable of performing microinjection on hundreds and thousands of cells per experiment. The system is embedded with strong automation capabilities in every step of operation, enabling an operator to perform the entire microinjection process via computer mouse clicking in front of a computer monitor. Training of a user with no skills in microinjection takes 10-15 minutes, and after a few hours' operation, the user becomes highly proficient at operating the system to perform adherent cell microinjection with high success rates.

V. CONCLUSION

This paper described a robotic adherent cell injection system equipped with several key technologies that were recently developed. These new techniques include automatically locating micropipette tips, robustly detecting the contact of micropipette tip with cell culturing surface and directly with cell membrane, and precisely compensating for accumulative positioning errors. The high degree of automation of the system enables users with no microinjection training to perform large-scale cell injection with high success rates. System operation speed, success rate, and cell viability rate were quantitatively evaluated. Dye transfer experiments were conducted on different cell lines to establish a powerful assay for characterizing cell gap junction functions.

REFERENCES

[1] T. Pawson, "Protein modules and signalling networks." *Nature*, vol. 373, no. 6515, pp. 573–80, Feb. 1995.

[2] P. Friedl and K. Wolf, "Tumour-cell invasion and migration: diversity and escape mechanisms." *Nat. Rev. Cancer*, vol. 3, no. 5, pp. 362–74, May 2003.

[3] I. Stefanová, J. R. Dorfman, and R. N. Germain, "Self-recognition promotes the foreign antigen sensitivity of naive T lymphocytes." *Nature*, vol. 420, no. 6914, pp. 429–34, Nov. 2002.

[4] K. M. Abdullah, G. Luthra, J. J. Bilski, S. A. Abdullah, L. P. Reynolds, D. A. Redmer, and A. T. Grazul-Bilska, "Cell-to-cell communication and expression of gap junctional proteins in human diabetic and nondiabetic skin fibroblasts: effects of basic fibroblast growth factor." *Endocrine*, vol. 10, no. 1, pp. 35–41, Feb. 1999.

[5] Z. Lu, X. Zhang, C. Leung, N. Esfandiari, R. F. Casper, and Y. Sun, "Robotic ICSI (intracytoplasmic sperm injection)." *IEEE Trans. Biomed. Eng.*, vol. 58, no. 7, pp. 2102–8, July 2011.

[6] H. B. Huang, D. Sun, S. Member, J. K. Mills, and S. H. Cheng, "Robotic cell injection system with position and force control: toward automatic batch biomanipulation," *IEEE Trans. Robot.*, vol. 25, no. 3, pp. 727–737, 2009.

[7] A. Pillarisetti, S. Member, M. Pekarev, A. D. Brooks, J. P. Desai, and A. Member, "Evaluating the effect of force feedback in cell injection," *IEEE Trans. Autom. Sci. Eng.*, vol. 4, no. 3, pp. 322–331, 2007.

[8] S. Lim, N. A. Zeenathul, M. L. Mohd Azmi, O. Abas Mazni, and O. Fauziah, "Effect of protein concentration and injection pressure in microinjection delivery of maltose binding protein into breast cancer cells," *Pertanika J. Sci. & Technol.*, vol. 19, no. 2, pp. 273–283, 2011.

[9] K. Viigipuu and P. Kallio, "Microinjection of living adherent cells by using a semi-automatic microinjection system." *Alternatives to laboratory animals : ATLA*, vol. 32, no. 4, pp. 417–23, Oct. 2004.

[10] W. Wang, Y. Sun, M. Zhang, R. Anderson, L. Langille, and W. Chan, "A system for high-speed microinjection of adherent cells." *Rev. Sci. Instrum.*, vol. 79, no. 10, p. 104302, Oct. 2008.

[11] Y. Sun, S. Duthaler, and B. J. Nelson, "Autofocusing in computer microscopy: selecting the optimal focus algorithm." *Microsc. Res. Tech.*, vol. 65, no. 3, pp. 139–49, Oct. 2004.

[12] J. Liu, Z. Gong, K. Tang, Z. Lu, and Y. Sun, "Locating end-effector tips in automated micromanipulation," *IEEE Trans. Robot. (Accepted for Publication)*.

[13] W. Wang, X. Liu, and Y. Sun, "Contact Detection in Microrobotic Manipulation," *Int. J. Robot. Res.*, vol. 26, no. 8, pp. 821–828, Aug. 2007.

[14] W. Martin, G. Zempel, D. Hülser, and K. Willecke, "Growth inhibition of oncogene-transformed rat fibroblasts by cocultured normal cells: relevance of metabolic cooperation mediated by gap junctions." *Cancer Res.*, vol. 51, no. 19, pp. 5348–51, Oct. 1991.

[15] R. M. Mège, D. Goudou, C. Giaume, M. Nicolet, and F. Rieger, "Is intercellular communication via gap junctions required for myoblast fusion?" *Cell Adhes. Commun.*, vol. 2, no. 4, pp. 329–343, Aug. 1994.

[16] T. Nishimura, C. Dunk, Y. Lu, X. Feng, a. Gellhaus, E. Winterhager, J. Rossant, and S. J. Lye, "Gap junctions are required for trophoblast proliferation in early human placental development." *Placenta*, vol. 25, no. 7, pp. 595–607, Aug. 2004.

[17] S. Rohr, "Role of gap junctions in the propagation of the cardiac action potential." *Cardiovasc. Res.*, vol. 62, no. 2, pp. 309–22, May 2004.

[18] J. W. Holder, E. Elmore, and J. C. Barrett, "Gap junction function and cancer." *Cancer Research*, vol. 53, no. 15, pp. 3475–85, Aug. 1993.

[19] T. K. Kim and J. H. Eberwine, "Mammalian cell transfection: the present and the future." *Anal. Bioanal. Chem.*, vol. 397, no. 8, pp. 3173–8, Aug. 2010.